TRANSPORT PROBLEMS 2023 Volume 18 Issue 1
PROBLEMY TRANSPORTU DOI: 10.20858/tp.2023.18.1.11

Keywords: railway track; ballast degradation; image extraction algorithm; surface descriptors

Piotr LESIAK[1]*, Piotr BOJARCZAK[2], Aleksander SOKOŁOWSKI[3]

ALGORITHM FOR THE EXTRACTION OF SELECTED RAIL TRACK BALLAST DEGRADATION USING MACHINE VISION

Summary. A number of physical methods are used to survey railway track ballast to assess its degradation as a function of deposition. Simulation tests on track models are also conducted. These testing methods, which are generally labour-intensive and expensive, provide an accurate understanding of the extent of ballast degradation. However, the impact of inadequate maintenance can be observed, even on the surface. Therefore, it seems natural in this case to use image registration. State-of-the-art machine vision systems of track geometry cars provide the means to do this. Obtained ballast images provide a baseline for evaluating its level in relation to sleepers. However, no information is available on other signs of track degradation, such as overgrown vegetation (weeds) or the so-called local muddy areas, which are generally a consequence of poor drainage and a lack of subgrade insulation. These degradations are observed to generate distinctive colour images that are superimposed on the overall image of the ballast surface. They differ in colour and shape. Hence, the authors used this phenomenon to develop an algorithm for the extraction of ballast degradation images based on RGB imaging. Surface descriptors have also been offered to assess these degradations. Extensive measurement material from the railway lines was used to conduct survey experiments based on the examples. The results clearly demonstrate the high success rate of the applied method.

1. INTRODUCTION

Conventional ballasted tracks formed from well-distributed crushed stone are used as the main structure for railway lines worldwide. The primary task is to absorb the thrust originating from a train and to distribute it over as large an area as possible, thereby providing appropriate cushioning and damping properties. The use of an appropriate track ballast is critical to the safe and smooth running of a train [28].

Despite these benefits of the ballast, it is important to anticipate its continuous degradation, such as abrasion and cracking under high cyclic load (which causes track deterioration) and permanent geometry deformation (which affects safety with a potential loss of track stability and requires frequent and costly maintenance). Geotechnical conditions affect degradation by causing the cementation and contamination of the ballast, the deposition of eroded materials, mud, and clay from the bedding upwards and the intrusion of coal. This leads to differences in subsidence and a reduction in the rigidity of the sleeper support by the deconsolidation of the ballast, thus changing the vibration characteristics [8, 11, 18, 35].

[1] WSEI University; Projektowa 4, 20-209 Lublin, Poland; e-mail: piotr.lesiak@wsei.lublin.pl; orcid.org/0000-0002-9792-3463
[2] Kazimierz Pulaski University of Technology and Humanities in Radom; Malczewskiego 29, 26-600 Radom, Poland; e-mail: p.bojarczak@uthrad.pl; orcid.org/0000-0002-1977-9865
[3] Rzeszów University of Technology; al. Powstańców Warszawy 12, 35-959 Rzeszów, Poland; e-mail: alex5@prz.edu.pl; orcid.org/0000-0002-1878-5382
* Corresponding author. E-mail: piotr.lesiak@wsei.lublin.pl

This is accompanied by reduced track drainage capacity. Over time, a track located on a wet bedding with cohesive soils that are not separated from the ballast by a protective covering will settle disproportionately further. Silt and clay particles are sucked up with water and carried into the ballast, and the train thrust transmitted to the sleepers acts as a pump. Therefore, the ballast gets contaminated with these fine particles, which form mud when wet and a hard crust when there is a dry period. Voids are also formed, making it less comfortable to travel. The maintenance of a wet bedding may involve the local replacement of the ballast. However, unless the underlying cause is addressed, the problem is likely to recur, requiring repeated maintenance operations. This is an expensive and relatively inefficient approach to dealing with the problem. Hence, it is advisable to install a geotextile filter and a geogrid [14, 16].

Therefore, it is essential to have an efficient monitoring system to enhance the maintenance of the railroad ballast, which entails periodic maintenance and repairs. These are labour-intensive and expensive operations, which are supported by intensive research work in this field [1, 12, 26, 31, 34].

There are two main approaches applied to help understand the mechanical behaviour of a railroad ballast that leads to its failure: experimentation and modelling [1-2]. Conventional laboratory sampling experiments have produced inaccurate results due to the large size of the ballast particles in relation to the sample size. Therefore, a non-invasive ballast test method with a ground penetrating radar (GPR) is commonly applied [29, 31]. It uses polarised high-frequency radio waves, usually in the range of several hundred MHz to several GHz. The GPR transmitter and antenna emit an electromagnetic wave into the railway subgrade. The boundary between materials of different permeability causes wave reflection, refraction or scattering. The structural image of the ballast and deeper layers of the subgrade obtained by GPR surveying identifies its degradation, particularly contamination, mud patches, and water stagnation, with expected increased wave suppression [20]. Therefore, this GPR measurement technique is particularly appropriate for railway track transition zones, where there are significant changes in the vertical structure of the track [36-37].

Enhanced signal processing algorithms, including bicubic interpolation, gain compensation, and reflection signal envelope extraction combined with background removal, have been implemented in the latest ultra-wideband GPR radar developments to effectively eliminate noise and interference, thereby improving the detection of ballast contamination [38].

A variation of the GPR is the spectral analysis of surface waves method, which is an in-situ seismic method for measuring the velocity of ballast transverse waves. The dispersive characteristics of Rayleigh waves are used here. As a result, Young's modulus is calculated for both clean and soiled ballasts under wet and dry conditions [32-33].

By using different approaches to modelling the properties of the ballast material, it is indeed feasible to aggregate the scanning areas, thus increasing the accuracy of the surveys, which ultimately leads to positive economic results and minimal maintenance and replacement costs [4].

For finite element method modelling, edge cracking at the sleeper/ballast contact is surveyed. Both edge cracking and particle movement in the ballast bed were found to affect the subsidence of the sleeper. These simulations, therefore, can aid the general understanding of micro-macro phenomena involving railway ballasts. This can help upgrade track components and track design based on simulation models that incorporate the physical behaviour of the ballast [6]. In modelling, the best results are obtained by conducting triaxial modelling [3].

Critical spots on a railway track include turnouts, where maintenance is a major cost factor for any infrastructure manager. Maintenance work is performed based on a preventive or periodic policy to minimise turnout downtime. Such areas pose a significant challenge to the ballast, as its degradation largely accounts for excessive failures of turnout components. The measurable extent of ballast degradation and packing, in this case, is the exceedance of turnout geometry standards, which is a predictor of their maintenance [7].

Therefore, models of ballast degradation are developed and compared based on regression analysis and stochastic processes (normal and gamma distributions). These models are developed for different sections of a single turnout, as well as for different turnouts with variable geographical locations [5].

Important signs of significant degradation of the ballast on the surface are vegetation overgrowth and the formation of local muddy areas (LMAs) characterised by mud pumping [22, 24].

PKP PLK S.A. classifies the condition of the ballast [17] as good with no LMAs, rarely visible weeds, full gravel pack of the longitudinal side of sleepers and no empty spaces under the sleepers (Fig. 1a).

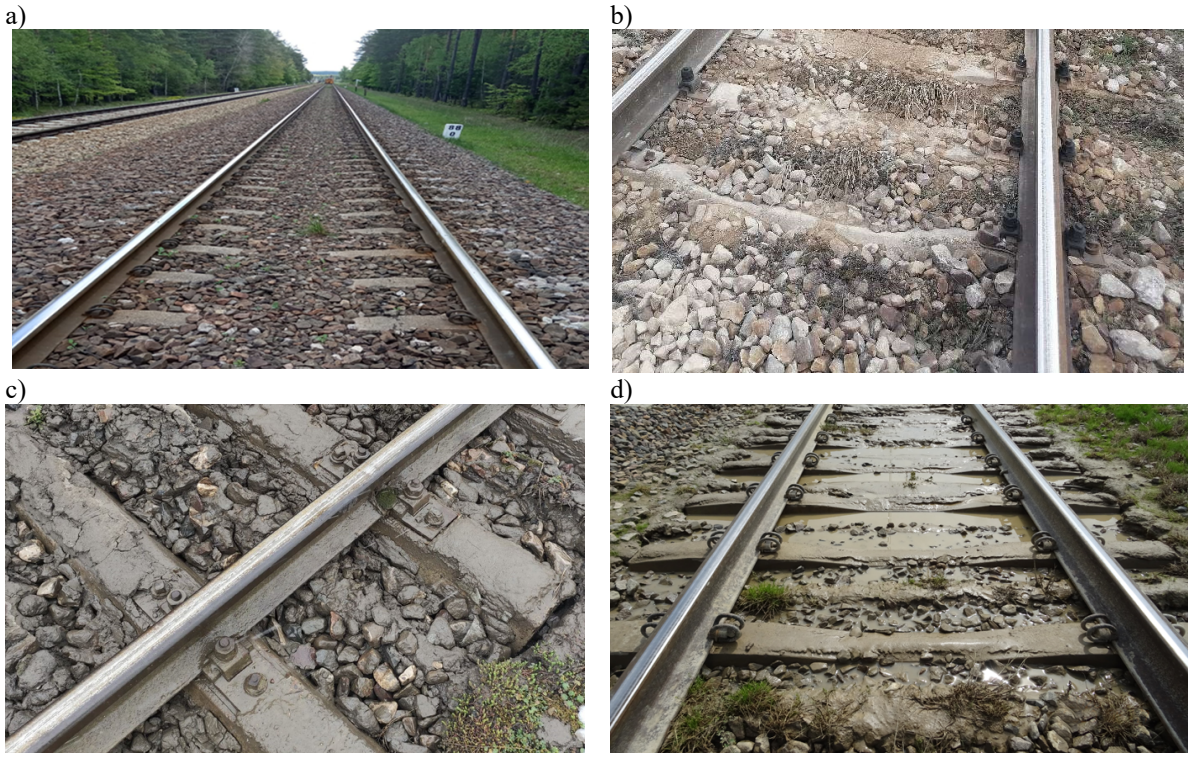

Fig. 1. Examples of track ballast degradation (authors' photos from the PLK and LHS lines): a) Good condition, line 65, Zwierzyniec – Biłgoraj route, b) average condition, line 61, Kielce – Fosowskie route, Małogoszcz station, c) poor condition, line 7, Lublin Towarowy station, and d) very poor condition, line 91, Kraków Główny – Medyka

An average condition means there are single LMAs on not more than two adjacent sleepers at amounts not exceeding 15% of the surface of the sleepers. There is also heavy weed infestation, and individual sleepers have their longitudinal sides exposed up to 2/3 of their height (Fig. 1b).

A poor condition means LMAs cover three to five consecutive sleepers at an amount of up to 30% of all sleepers. There is also potential heavy weed infestation and a lack of ballast between sleepers up to 2/3 of their height (Fig. 1c).

A ballast in very poor condition means the LMAs cover more than five consecutive sleepers at an amount greater than 30% of all sleepers; there are also voids between sleepers and completely exposed longitudinal sides of sleepers over a length of more than 4 m (Fig. 1d).

Therefore, it seems obvious in this case to use image registration of the ballast. This is enabled by the modern machine vision systems of track geometry cars.

In standard surveying solutions of machine vision systems equipped with cameras installed on rail vehicles (motor cars), the detection, segmentation, recognition, and evaluation of defects of railway track components, including turnouts, is performed. These include defects in rails, their fastenings and joints, and cracks in the sleepers [25].

Owing to the important role of the ballast in rail track maintenance, diagnostic options have been supplemented with a system that registers colour images of the ballast, including light detection and ranging, by which a laser beam illuminates the track and a camera records the image of the reflection from the ballast (surface map). This forms the basis for evaluating level the ballast against the sleepers, allowing faster and more accurate maintenance [27, 38].

These systems do not have algorithms that provide information regarding the recognition of the indicated symptoms of ballast degradation, namely vegetation and LMAs, which is the main objective of the authors' considerations.

2. MOBILE MEASURING SYSTEM

During the survey, the authors applied vision data recorded by a specialised vehicle (motor car) equipped with a mobile diagnostic laboratory for the comprehensive evaluation of railway lines, Fig. 2a.

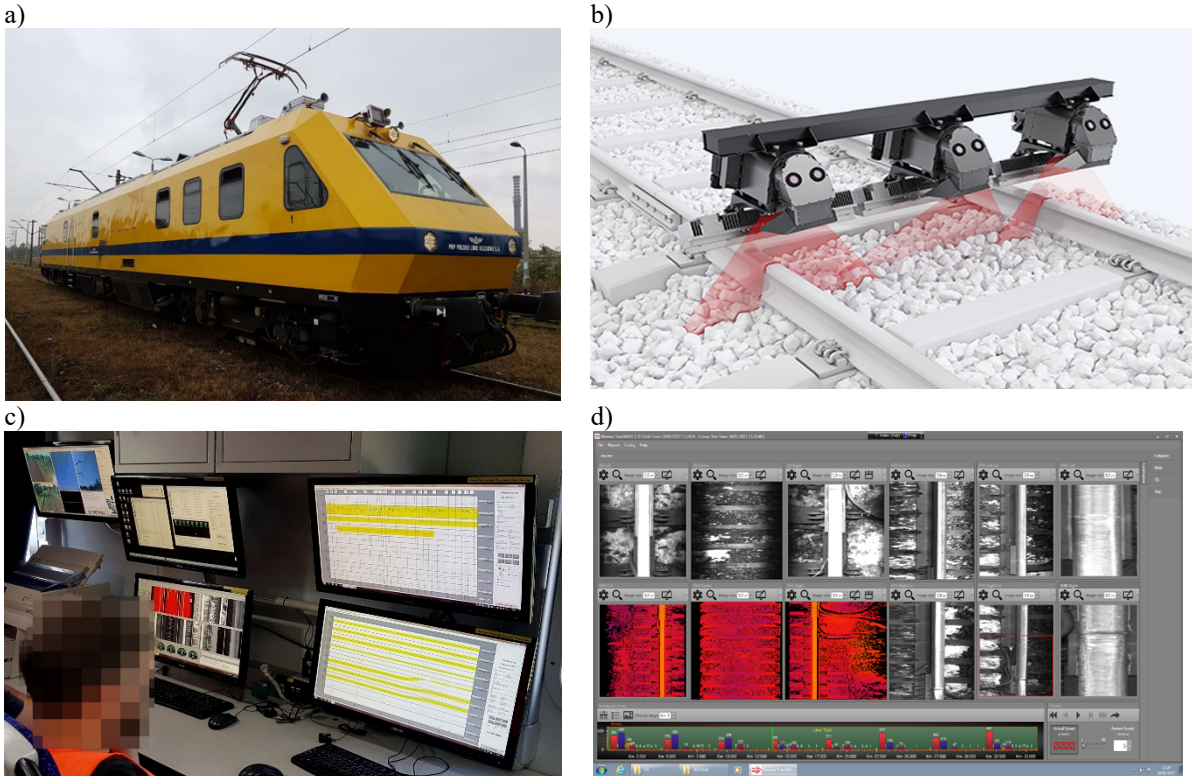

Fig. 2. Track geometry car type DP-560 -01 of PKP PLK S.A.: a) A general view, b) a V-CUBE laser system, c) a view of measurement and machine vision displays, and d) a ballast visualisation display (red colour)

With lasers and camera units, system provides a track bed check to measure the geometry of the track and rails, check the condition of sleepers (cracks) and ballast (level), and even perform catenary diagnostics, as shown in Fig. 2c.

Cameras on the vehicle register the railway route and allow faults to be detected quickly. Non-contact laser systems enable measurements to be taken without affecting railway signalling systems; thus, train traffic on the network is not restricted.

The vehicle, which had been operated for about two years by the PKP PLK S.A. Diagnostic Centre, was equipped with measuring equipment by the Italian company Mermec [23]. The equipment is capable of surveying around 40,000 kilometres of track per year at a maximum speed of 120 km/h, thereby collecting tens of terabytes of diagnostic data.

Structurally, the vehicle is suspended on 2 two-axle bogies with pneumatic suspension units. This has a significant impact, above all, on the correct measurement results. It is also equipped with the ETCS Level 2 system.

The vehicle running gear uses the V-CUBE universal laser system (Fig. 2b). This system is able to capture images from measurements in the speed range from 0 to 200 km/h from three different subsystems, thus providing a complete check of the track infrastructure. It automatically identifies more than 50 different types of defects, including those on the running surface of rails, their fastenings, sleepers, and (the main area of interest for the authors) the subgrade (Fig. 2d). Due to the specific system and the construction of the equipment, the ballast shoulder is not recorded. Such research would require a completely different measurement method; as with the current train, the limits of rolling stock would be exceeded.

3. ALGORITHM FOR VEGETATION AND LMA EXTRACTION FROM BALLAST IMAGES

In medicine [10, 40] as well as in agriculture [13, 19], one can find algorithms that use colour intensity distributions to detect desired objects such as tumours or crop areas. The authors have used similar methods for vegetation and LMA extraction from ballast images.

The algorithm applies the RGB colour space model, which uses 24-bit colours (8 bits for each of the component colours). Each colour is saved with components that assume a value in the 0-255 range. In the RGB model, values of 0 of all components produce black, while values of 255 produce white.

The colour intensity distribution of images of a railway track ballast degraded by areas of vegetation (weeds) and LMAs can be represented by the following function:

$$f(x, y, \nu_R, \nu_G, \nu_B) = \iiint_{N_{R'}N_{G'}N_{B'}} g\,(x, y, \nu_R, \nu_G, \nu_B)\delta(\nu_R - \nu_{R'})\delta(\nu_G - \nu_{G'})\delta(\nu_B - \nu_{B'})d\nu_{R'}d\nu_{G'}d\nu_{B'} \quad , \tag{1}$$

where ν_R, ν_G, ν_B – the colour components in the RGB model of a given point in the plane of the image in question and $\nu_{R'}, \nu_{G'}, \nu_{B'}$ – the colour components in the area of vegetation or LMAs (integration is performed after these components).

Integration after $N_{R'}, N_{G'}, N_{B'}$ is performed after colours intensify in an area limited to the ambient area of a particular colour. δ represents the Dirac delta distribution.

Actual images are described as sets of pixels, each with coordinates and an assigned colour. Thus, formula (1), in a discrete form, assumes the following form:

$$\phi(\xi_i, \psi_i, \nu_{vP}, \nu_{vB}, \nu_{vT}) = \sum_{N_{R'}} \sum_{N_{G'}} \sum_{N_{B'}} g\,(x_i, y_i, n_R, n_G, n_B)\delta_{n_R,n_{R'}}\delta_{n_G,n_{G'}}\delta_{n_B,n_{B'}} \quad , \tag{2}$$

where the integration in Formula (1) has been replaced by aggregation after the colour intensities of the individual pixels. The Dirac delta functions have been replaced by Kronecker symbols.

Aggregating after $N_{R'}, N_{G'}, N_{B'}$ for the selected colour, as described by the triple $n_{R'}$, $n_{G'}$, and $n_{B'}$ and assuming the colour bandwidth where the pixels have a non-zero value, the following intervals are obtained: $[n_{R'} - \Delta n_{R'}, n_{R'} + \Delta n_{R'}]$, $[n_{G'} - \Delta n_{G'}, n_{G'} + \Delta n_{G'}]$, and $[n_{B'} - \Delta n_{B'}, n_{B'} + \Delta n_{B'}]$.

If a given pixel has a colour within these intervals, it will retain its colour; otherwise, the colour will be zero (black).

The extraction procedure for vegetation areas or LMAs has been developed by one of the co-authors in the Delphi program. An example is shown in Fig. 3a, in which the original ballast image, contaminated with vegetation (weeds), as registered by the vehicle machine vision system, is displayed.

First, a pixel of a specific colour is selected – in Fig. 3a, it is yellow, representing vegetation growing above the track level – and a procedure is launched to select colours within the described intervals. If the pixel colour is outside these intervals, it assumes a value of zero (i.e., black is added), as shown in Fig. 3b. Of course, the width of these intervals matters for the extraction of the corresponding image areas. Figs. 3b and 3c show images of different values of the parameter $\Delta n_{x'}$, assuming that $\Delta n_{R'} = \Delta n_{G'} = \Delta n_{B'} = \Delta n$. Fig. 3b shows the image obtained for $\Delta n = 10$, and Fig. 3c shows the image obtained for $\Delta n = 40$.

If the algorithm does not cover all the colours corresponding to vegetation, as shown in Fig. 3a, in which white and dark yellow also appear, it seems natural to complete the procedure for these colours, as shown in Figs. 4a and 4b. The superposition of these images for $\Delta n = 40$ resulted in the image depicted

in Fig. 4c. The full vegetation image shown in Fig. 4d was obtained when supplemented by the image from Fig. 3c, which realistically corresponds to its extraction from Fig. 3a, as highlighted by their 3D images in Fig. 5.

Of course, the number of aggregated partial images assigned to each colour can be variable and depends on their shades, usually from one to four, as in the example with vegetation shown above.

Further experiments on the operation of the algorithm were performed for LMAs, where almost continuous coherent ballast areas are visible without differentiating (discretising) the stones.

The first LMA piece is level with the top surface of the sleepers (red), and the second is below this surface (purple), as shown in Fig. 6a. Fig. 6b highlights the red colour of the image, and Fig. 6c highlights the purple colour, which is the second piece of the LMA image. The yellow-orange stones in Fig. 6a (in the area of the final image from Fig. 5d) are depicted as black holes.

After applying superposition for vegetation, a full image of the LMA in the area of the four sleepers was obtained (Fig. 6d). Unlike the example with vegetation, this image is limited to two colours.

The images obtained with this method show that the method is effective. Good extraction of the selected colours, corresponding vegetation (weeds), LMAs, and other ballast contamination sources resulting from the operation of rail vehicles is achievable.

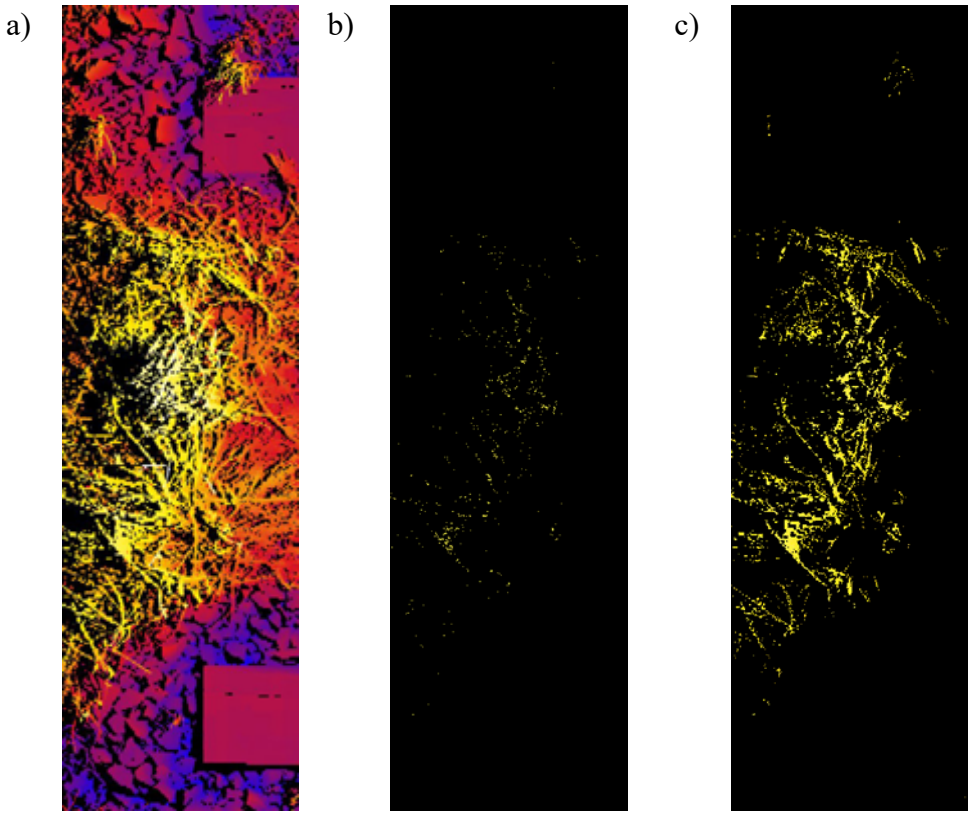

Fig. 3. An example of how the ballast vegetation extraction algorithm works for yellow colour: a) The original image, b) the image for $\Delta n = 10$, and c) the image for $\Delta n = 40$

4. SURFACE DESCRIPTORS IN THE EVALUATION OF DEGRADED BALLAST IMAGES

Using the algorithm suggested by the authors, an attempt was made to determine the key descriptors of the images (degraded ballast areas) as defined in the co-author's work [21]. PKP PLK S.A. does not precisely define its degradation criteria upon image analysis but only characterises them descriptively, as presented in point 1. Therefore, the authors considered that the most natural measure would be the

geometric surface descriptors of ballast areas with poor maintenance, degraded vegetation (weeds), or LMAs.

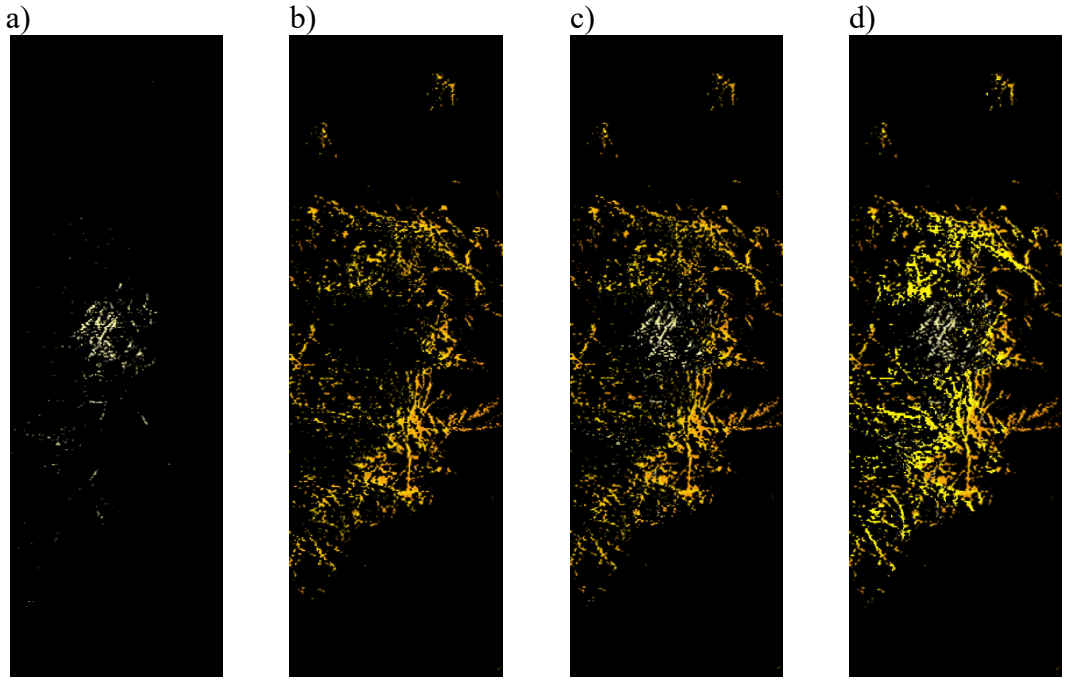

Fig. 4. Example of the superposition of the operation of the ballast vegetation extraction algorithm: a) a white image from 3a, b) an orange image from 3a, c) an aggregate of the images from 4a and 4b, and d) an aggregate of the images in 4c and 3c

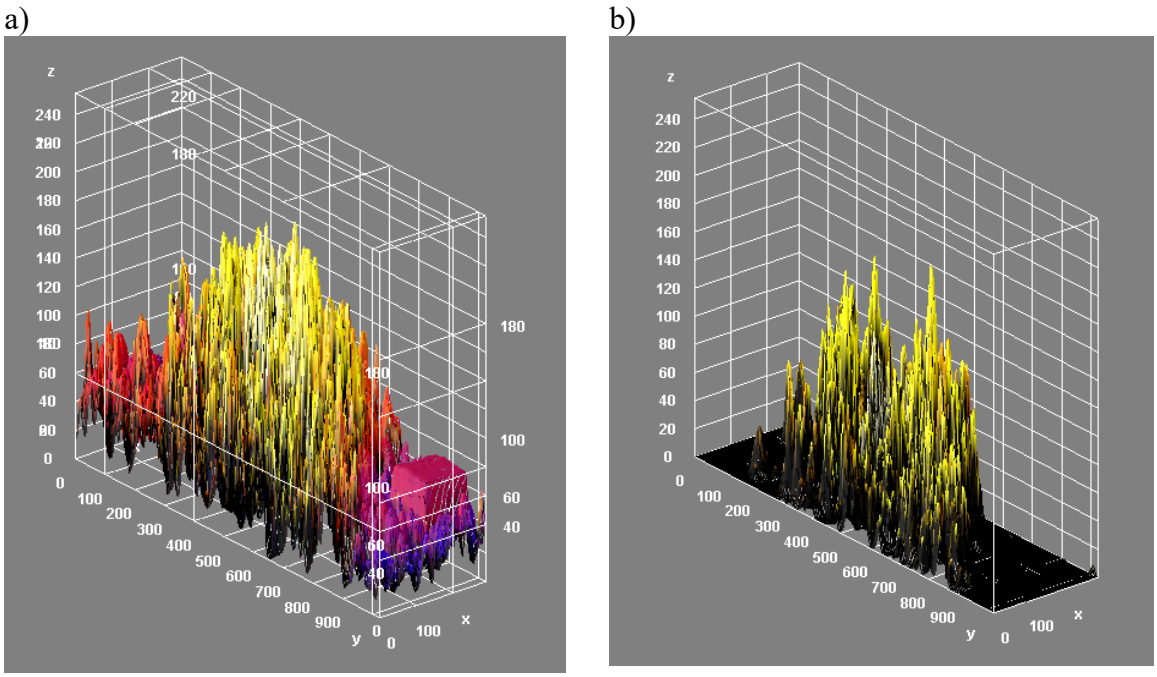

Fig. 5. 3D images of ballast vegetation: a) The original image from Fig. 3a and b) the image after extraction of vegetation from Fig. 4d

The descriptor calculations provided by the ImageJ program (Image Processing and Analysis in Java) were used [9, 15].

The program is written in Java and works with 8-, 16- or 32-bit greyscale images, as well as 24-bit colour images. It performs most of the standard image processing operations, as well as basic measurements and analysis, to be used in assessing the ballast condition.

The analysis was based on the simultaneous thresholding of RGB colour images in three channels, which was performed in the ImageJ program using the Threshold Color function (Fig. 7a). The LMA examples in Fig. 6d and the vegetation examples in Fig. 4d were used by applying the mean thresholding method. Conversion into B&W images yielded the images shown in Figs. 7d and 7e. Choosing a different method entails a change in the image after thresholding and, consequently, in the values of the descriptors determined, as described extensively in [30].

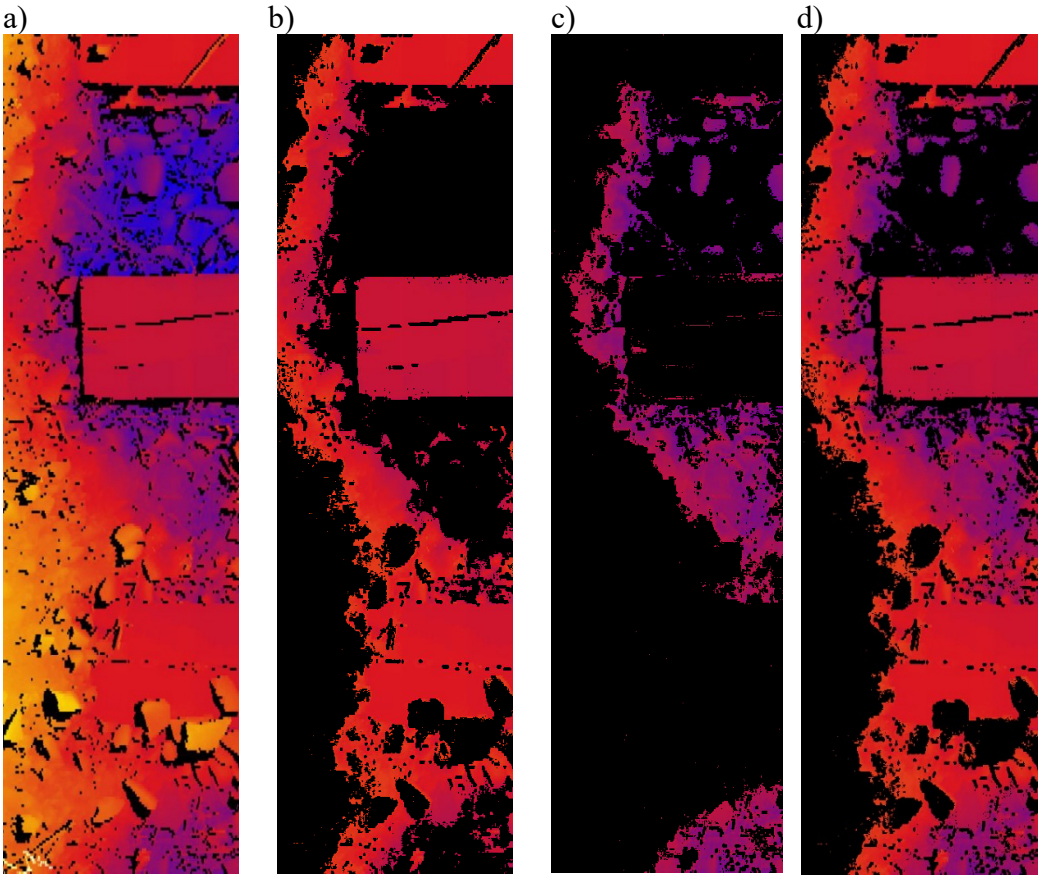

Fig. 6. Images for an LMA: a) The original image, b) the image after selecting red from 6a, c) the image after selecting violet from 6a, and d) the image after totalling 6b and 6c

The choice of descriptors is made in the Set Measurement window (Fig. 7b). Fig. 7c specifies the size and circularity ranges of the areas considered when computing the descriptors. The total area of a single sample is 288x1024=294,912 pixels.

By converting the RGB image of the ballast area degradation $d(m,n)$ into a binary image (1 and 0 correspond to the points belonging to the degraded and non-degraded areas, respectively), with a sample size of MN pixels for LMAs in Fig. 6d or the vegetation shown in Fig. 6e, their area can be defined as follows [21]:

$$A_d = \sum_{m=0}^{M-1} \sum_{n=0}^{N-1} d(m,n) \quad . \tag{3}$$

On the other hand, using the threshold criterion, the ratio of the degraded ballast area to the maximum value of the aggregate of the pixel amplitudes in the entire sample area can be determined (i.e., $255\ MN$). For the assumed threshold T_d, a check is made to ensure that it does not exceed an arbitrarily assumed value:

$$T_d = \frac{A_d}{255MN} 100\% \quad . \tag{4}$$

Using the example of the extracted LMA from Fig. 6d, the area fraction of this degradation (59%) was obtained in the total area of the sample image. This can be used as the main criterion for assessing damage to the track ballast, assuming, for example, a limit value of 50%. An increase in the degradation area, brought about by the sleepers, has to be accounted for (Fig. 7d).

Similarly, a 12% area of degradation was obtained for the vegetation in Fig. 4d. In this case, the area of the sleepers is irrelevant, as their colour is significantly distant from the weeds protruding above the surface.

The image degradation centre, in turn, is defined by a pair of coordinates, $\overline{m}, \overline{n}$ [21]:

$$\overline{m} = \frac{1}{A_d}\sum_{m=0}^{M-1}\sum_{n=0}^{N-1} md(m,n), \overline{n} = \frac{1}{A_d}\sum_{m=0}^{M-1}\sum_{n=0}^{N-1} nd(m,n) \quad . \tag{5}$$

This description helps locate degradations in the two-dimensional image plane. In the example of the LMA in Fig. 7d, $\overline{m}$ =128 and $\overline{n}$ =523. For the vegetation in Fig. 7e, $\overline{m}$ = 147 and $\overline{n}$ =519.

By evaluating the shape and position of the ballast degradation in the surveyed sample image, shape descriptors, which provide information about the shape and orientation of the degraded image, were also determined. The skewness descriptor, defined as the angle Θ to the axis Y at the centre of the area $\overline{m}, \overline{n}$, can be determined from the following expression:

$$tg(2\Theta) = 2\frac{\sum_{m=0}^{M-1}\sum_{n=0}^{N-1} mnd(m,n)}{\sum_{m=0}^{M-1}\sum_{n=0}^{N-1} m^2 d(m,n) - \sum_{m=0}^{M-1}\sum_{n=0}^{N-1} n^2 d(m,n)} \tag{6}$$

For the LMA, the skewness descriptor was $\Theta \sim 28^0$, and for the vegetation, the skewness descriptor was $\Theta \sim 10^0$, as the degradation images deviate little from the vertical axis.

Knowing the image perimeter $\overline{O}_d$ of the ballast degradation area allows another shape descriptor to be determined. In a binary image, the image perimeter can be determined by counting the number of pixels described as "1" that have adjacent pixels described as "0." Once the perimeter $\overline{O}_d$ and area A_d have been found, the so-called thinness factor, which is a measure of roundness, is calculated:

$$l = 4\Pi\left(\frac{A_d}{\overline{O}_d^{\,2}}\right) \quad . \tag{7}$$

The closer this value is to 1, the more the image resembles a circle. Should the perimeter become larger compared to the surface area, this ratio decreases, and the image becomes thinner. In the examples shown in Figs. 7d and 7e, the roundness is about 0.28.

The degradation shape can also be evaluated by Fit Ellipse; this program includes the outer edges of the entire sample. Thus, in the examples, the axes extend beyond the sample area. The dimension of the minor axis is 324 pixels and the major axis is 1155 pixels.

As a result of further surveys, such descriptor values were obtained for LMAs and vegetation, respectively, as follows [30]: mean – 151 and 29, standard deviation – 125 and 63, minimum and maximum grey values – 0 and 255, and median – 255 due to the predominant number of image pixels at level 1 (white) and 0 (black) for weeds.

Using the ImageJ Analyze Particles function, a detailed analysis of measurements of separated image fractions in the degradation area can be performed; thus, shape selection depends on size and roundness (Fig. 7c). In the example shown in Fig. 7d, the LMA area was divided into fractions containing 1 to 1953 pixels, and the ranged from 1 to 817 (Fig. 7e).

When extracting fragments from an image, each successively extracted fragment is assigned another number. Fig. 8a shows the relationship between the area of an extracted image fragment and its assigned number for the example vegetation samples in Fig. 7e. The extraction process yielded five fragments (fragment numbers 64, 293, 323, 429, and 613) with the largest area. Fig. 8b shows the dependence of the median pixel intensity occurring in the extracted fragment on the number assigned to it for the same samples in Fig. 7e. Its minimum value is 21, and its maximum value is 185.

The function also allows pixels bordering the edge of the image to be excluded (Exclude on Edges), which provides more reliable measurements of individual parts of the image.

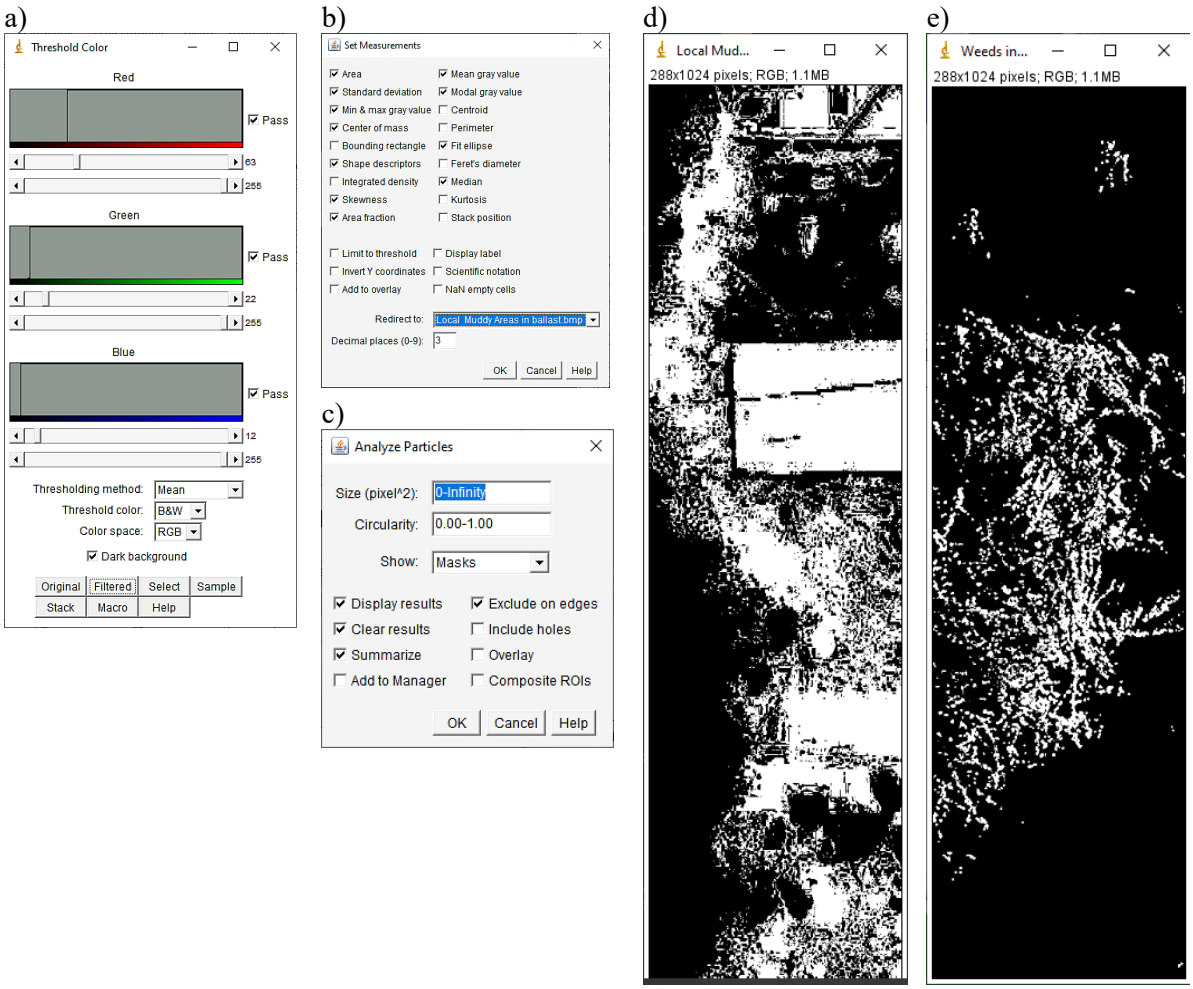

Fig. 7. Image measurement parameters: a) A thresholding application window, b) and c) measurement windows and images after thresholding, d) LMAs from Fig. 6d, and e) the vegetation from Fig. 4d

5. CONCLUSIONS AND FURTHER WORK

The present survey demonstrates the feasibility of using RGB colour images to extract ballast degradation, such as vegetation (weeds) and LMAs. This method, along with ballast evaluation based on surface descriptors, provides a simple and intuitive pathway for indicating locations on a track where there is a need for immediate maintenance operations without the need to conduct the complex surveys presented in the introduction of this work.

Additionally, the descriptors used in this work make it possible to define the features of the selected areas. This allows for a qualitative comparison of the areas extracted by the algorithm.

The track visualisation recently used in diagnostic surveys using high-resolution cameras in the track geometry cars creates the proper framework for this process.

The authors anticipate that in further work, it would be desirable to involve more sophisticated methods based on deep learning networks. The result is expected to be high-quality image processing and recognition algorithms that provide comprehensive railway track diagnostics.

Acknowledgements

The authors would like to thank Mr Ludwik Madej, head of the Diagnostic Measurements Department of the Office of the Diagnostic Centre of PKP Polskie Linie Kolejowe S.A., for providing the images from the ballast survey.

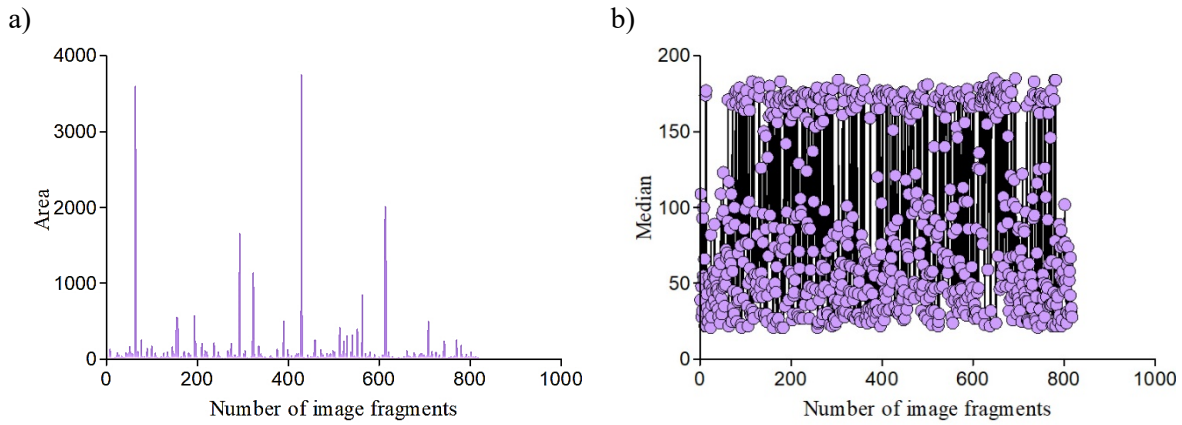

Fig. 8. Illustration of the relationships between the extracted vegetation image fragments from Fig. 7e for their a) area and b) median pixel brightness

References

1. Adeagbo, M.O. & Lam, H.F. & Hu, Q. On the selection of the most plausible non-linear axial stress – strain model for railway ballast under different impulse magnitudes. *Structural Health Monitoring.* 2021. Vol. 21(4). P. 1447-1473. DOI: https://doi.org/10.1177/14759217211033968.
2. Alabbasi, Y. & Hussein, M. Geomechanical modelling of railroad ballast: a review. *Archives of Computational Methods in Engineering.* 2021. Vol. 28. P. 815-839. DOI: https://doi.org/10.1007/s11831-019-09390-4.
3. Alabbasi, Y. & Hussein, M. Large-scale triaxial and box testing on railroad ballast: a review. *SN Applied Sciences.* 2019. Vol. 1. Article number: 1592. DOI: https://doi.org/10.1007/s42452-019-1459-3.
4. Alemu, A.Y. *Survey of Railway Ballast Selection and Aspects of Modelling Techniques*. Department of Transport Science. School of Architecture and the Built Environment, Royal Institute of Technology. SE-100 44. Stockholm. 2011. 61 p.
5. Asadzadeh, S.M. & Galeazzi, R. & Hovad, E. & Andersen, J.F. & Thyregod, C. & Rodrigues, A.F.S. Ballast degradation modelling for turnouts based on track recording car. *Data Proceedings of the European Conference of the Prognostics and Health Management Society.* 2018. Vol. 4(1).
6. Bach, H. Evalua*tion of attrition tests for railway ballast.* Graz University of Technology. Institute for Railway Engineering and Transport Economy. Dissertation. 2013. 111 p.
7. Barkhordari, P. & Galeazzi, R. & Blanke, M. Prognosis of railway ballast degradation for turnouts using track-side accelerations. *Proceedings of the Institution of Mechanical Engineers, Part O: Journal of Risk and Reliability.* 2020. Vol. 234(4). DOI: https://doi.org/10.1177/1748006x20901410.
8. Bassey, D. & Ngene, B. & Akinwumi, I. & Akpan, V. & Bamigboye, G. Ballast contamination mechanisms: a criterial review of characterisation and performance indicators. *Infrastructures.* 2020. Vol. 5(11). DOI: https://doi.org/10.3390/infrastructures5110094.
9. Burger, W. & Burge, M.J. Principles of digital image processing. Advanced methods. Vol. 3. *Undergraduate Topics in Computer Science*. Springer-Verlag. London, 2013. 43 p.
10. Chen, J. & Stanley, R.J. & Moss, R.H. & Stoecker, W.V. Color analysis of skin lesion regions for melanoma discrimination in clinical images. *Skin Research & Technology.* 2003. Vol.9(2). P. 94-104. DOI: https://doi.org/10.1034/j.1600-0846.2003.00024.x.
11. Dalberg, T. Modelling of the dynamic behavior of in situ concrete railway sleepers. *Proceedings of the Institution of Mechanical Engineers Part F: Journal of Rail and Rapid Transit*. 2008. Vol. 222(4). P. 433-440.

12. Guerrieri, M. & Parla, G. & Celauro, C. Digital image analysis technique for measuring railway track defects and ballast gradation. *Measurement.* 2018. Vol. 113. P. 137-147. DOI: https://doi.org/10.1016/j.measurement.2017.08.040.
13. Hassanein, M. & Lari, Z. & El-Sheimy, N. A new vegetation segmentation approach for cropped fields based on threshold detection from hue histograms. *Sensors* 2018. Vol.18(4). P. 1253. DOI: https://doi.org/10.3390/s18041253.
14. Hudson, A. & Watson, G. & Pen, L.L. & Powrie, W. Remediation of mud pumping on a ballasted railway track. *Advances in Transportation Geotechnics 3. The 3rd International Conference on Transportation Geotechnics (ICTG 2016). Procedia Engineering*. 2016. Vol. 143. P. 1043-1050. DOI: https://doi.org/10.1016/j.proeng.2016.06.103.
15. ImageJ. Available at: https://imagej.nih.gov/ij/.
16. Indraratna, B. & Salim, W. & Rujikiatkamjorn, C. *Advanced Rail Geotechnology - Ballasted Track*. CRC Press. 2011. 413 p.
17. *Instrukcja o dokonywaniu pomiarów, badań i oceny stanu torów Id-14 (D-75). Załącznik nr 4a, stan na dzień 1 marca 2010*. [In Polish: *Instruction for measurements, testing and track condition assessment Id-14 (D-75). Annex No. 4a, as per 1 March 2010*]. PKP Polskie Linie Kolejowe S.A.
18. Lam, H.F. & Wong, M.T. Railway Ballast Diagnose through Impact Hammer Test. *Procedia Engineering.* 2011. Vol. 14. P. 185-194.
19. Lauko, I.G. & Honts, A. & Beihoff, J. & Rupprecht, S. Local color and morphological image feature based vegetation identification and its application to human environment street view vegetation mapping, or how green is our county? *Geo-Spatial Information Science.* 2020. Vol. 23(3). P. 222-236. DOI: https://doi.org/10.1080/10095020.2020.1805367.
20. Leng, Z. & Al-Qadi, I.L. Railroad ballast evaluation using ground-penetrating radar: Laboratory investigation and field validation. Transportation Research Record: *Journal of the Transportation Research Board.* 2159. 2010. P. 110-117. DOI: https://doi.org/10.3141/2159-14.
21. Lesiak, P. & Bojarczak, P. *Przetwarzanie i analiza obrazów w wybranych badaniach defektoskopowych.* [In Polish: *Image processing and analysis in selected flaw detections*]. ITE-PIB Radom. 2012. 185 P.
22. Li, D. & Wilk, S. Recent studies on railway-track substructure at TTCI. *Transportation Safety and Environment.* 2021. Vol. 3(1). P. 36-49. DOI: https://doi.org/10.1093/tse/tdaa031.
23. MERMEC. Available at: https://www.mermecgroup.com/.
24. Nguyen, T.T. & Indraratna, B. Rail track degradation under mud pumping evaluated through site and laboratory investigations. *International Journal of Rail Transportation.* 2021. Vol. 10(1). P. 44-71. DOI: https://doi.org/10.1080/23248378.2021.1878947.
25. Resendiz, E. & Hart, J.M. & Ahuja, N. Automated visual inspection of railroad tracks. *IEEE Transactions on Intelligent Transportation Systems.* 2013. Vol. 14(2). P. 751-760. DOI: https://doi.org/10.1109/TITS.2012.2236555.
26. Sadeghi, J.M. & Emad, M. & Zakeri, J.A. Development of integrated railway ballast quality index. *International Journal of Pavement Engineering.* 2021. Vol. 22(1). P. 32-40.
27. Sadeghi, J. & Najar, M.E.M. & Zakeri, J.A. & Kuttelwascher, C. Development of railway ballast geometry index using automated measurement system. *Measurement*. 2019. Vol. 138. P. 132-142. DOI: https://doi.org/10.1016/j.measurement.2019.01.092.
28. Sadeghi, J.M. & Zakeri, J.A. & Najar, M.E.M. developing track ballast characteristic guideline in order to evaluate its performance. *IJR International Journal of Railway.* 2016. Vol. 9(2). P. 27-35. DOI: https://doi.org/10.7782/IJR.2016.9.2.027.
29. Scanlan, K.M. *Evaluating degraded ballast and track geometry variability along a Canadian freight railroad through ballast maintenance records and ground-penetrating radar*. Civil and Environmental Engineering University of Alberta. 2018. 240 p.
30. Sezgin, M. & Sankur, B. Survey over image thresholding techniques and quantitative performance evaluation. *Journal of Electronic Imaging.* 2004. Vol. 13(1). P. 146-165. DOI: https://doi.org/10.1117/1.1631315.

31. Silvast, M. & Nurmikolu, A. & Wiljanen, B. & Levomaki, M. An inspection of railway ballast quality using ground penetrating radar in Finland**.** *Proceedings of the Institution of Mechanical Engineers. Part F: Journal of Rail and Rapid Transit*. 2010. Vol. 224 (50). P. 345-351.
32. Stark, T.D. & Wilk, S.T. & Thompson, H.B. & Sussmann, T. Evaluating fouled ballast using seismic surface waves. *Proceedings of the 2016 Joint Rail Conference.* April 12-15. Columbia, South Carolina, USA. JRC2016-5714. 2016. DOI: https://doi.org/10.1115/JRC2016-5714.
33. Sussmann, Jr, T.R. & Thompson II H.B. & Stark, T.D. & Wilk, S.T. & Ho, C.L. Use of seismic surface wave testing to assess track substructure condition. *Construction and Building Materials*. 2017. Vol. 155. P. 1250-1255. DOI: https://doi.org/10.1016/j.conbuildmat.2017.02.077.
34. Sysyn, M. & Kovalchuk, V. & Gerber, U. & Nabochenko, O. & Pentsak, A. Experimental study of railway ballast consolidation inhomogeneity under vibration loading. *An International Journal for Engineering and Information Sciences*. 2020. Vol. 15(1). P. 27-36.
35. Sysyn, M. & Kovalchuk, V. & Gerber, U. & Nabochenko, O. & Parneta, B. Laboratory evaluation of railway ballast consolidation by the non-destructive testing. *Communications - Scientific Letters of the University of Zilina.* 2019. Vol. 21(2). P. 81-88. DOI: https://doi.org/10.26552/com.C.2019.2.81-88.
36. Wang, H. & Silvast, M. & Markine, V. & Wiljanen, B. Analysis of the dynamic wheel loads in railway transition zones considering the moisture condition of the ballast and subballast. *Applied Sciences*. 2017. Vol. 7(12). P. 1-18. DOI: https://doi.org/10.3390/app7121208.
37. Wang, S. & Liu, G. & Jing, G. & Feng, Q. & Liu, H. & Guo, Y. State-of-the-art review of ground penetrating radar (GPR) applications for railway ballast inspection. *Sensors*. 2022. Vol. 22(7). DOI: https://doi.org/10.3390/s22072450.
38. Zarembski, A.M. & Grissom, G.T. & Euston, T.L. On the use of ballast inspection technology for the management of track substructure. *Transportation Infrastructure Geotechnology.* 2014. Vol. 1. P. 83-109. DOI: https://doi.org/10.1007/s40515-014-0004-5.
39. Zhang, Y. & Venkatachalam, A.S. & Xia, T. & Xie, Y. & Wang, G. Data analysis technique to leverage ground penetrating radar ballast inspection performance. *IEEE Radar Conference.* Cincinnati, OH, USA. 19-23 May 2014. P. 463-468. DOI: https://doi.org/10.1109/RADAR.2014.6875636.
40. Yu, B. & Chen, W. & Zhong, Q. & Zhang, H. Specular highlight detection based on color distribution for endoscopic images. *Frontiers in Physics.* 2020. Vol. 8. DOI: https://doi.org/10.3389/fphy.2020.616930.

Received 02.10.2021; accepted in revised form 02.03.2023